Asymmetries of local arsenic bonding sites in As_xS_{1-x} and As_xSe_{1-x} glasses

T. Su,[1,*] P. Hari,[2] E. Ahn,[1] P. C. Taylor,[1] P. L. Kuhns,[3] W. G. Moulton,[3] and N. S. Sullivan[4]
[1]*Department of Physics, University of Utah, Salt Lake City, Utah 84112*
[2]*Department of Physics, California State University, Fresno, California 93740*
[3]*National High Magnetic Field Laboratory, Tallahassee, Florida 32306*
[4]*Physics Department, University of Florida, Gainesville, Florida 32611*
(Received 27 August 2002; published 18 February 2003)

We simulate high-field ^{75}As NMR line shapes by numerically diagonalizing the full Hamiltonian in the laboratory frame. The results of high field ^{75}As NMR in both glassy and polycrystalline As_xS_{1-x} and As_xSe_{1-x} binary systems are analyzed using this more accurate line-shape simulation. We find that for $x=0.4$ the asymmetry parameters of the electric-field gradient at As sites are less than 0.2 in both glassy and the polycrystalline samples, revealing the similarity of the local order in these two materials. In the glasses, we also find evidence of the influence of statistical fluctuations on the various bonding configurations, even at the stoichiometric concentrations.

DOI: 10.1103/PhysRevB.67.085203 PACS number(s): 71.55.Jv, 71.55.Gs, 73.61.Jc, 87.64.Hd

I. INTRODUCTION

Chalcogenide glasses refer to glasses that contain chalcogen atoms, such as sulfur (S), selenium (Se), or tellurium (Te). In addition to their potential technological applications, these glasses are of interest as prototypical materials for studying metastable changes in structural properties.[1,2] Also, these materials exhibit the so-called ''photodarkening effect,'' which is a metastable shift of the optical absorption edge to lower energy after extended exposure to light whose energy is at or above the optical band-gap energy.[3,4] Although this effect is closely related to the structural properties of the glasses, no detailed understanding currently exists. For these glassy materials, scattering techniques, such as x-ray-diffraction and Raman scattering, provide incomplete information about the local bonding arrangements. In addition, ^{75}As nuclear quadrupole resonance (NQR),[5–8] Zeeman perturbed NQR,[9] and nuclear magnetic resonance[10] (NMR) have been extensively used to study local order in the chalcogenide glasses. These techniques detect the electric-field gradient (EFG) produced at the As sites by the valence electrons. The coupling between the EFG tensor and the nuclear quadrupole moment of the As nuclei causes a splitting of the nuclear-spin energy levels, which can be detected by NQR, Zeeman perturbed NQR, or NMR. Since the EFG is sensitive to the local bonding arrangements, these techniques provide information on the local order that cannot be obtained from scattering techniques. To extract the bonding arrangements, Zeeman perturbed ^{75}As NQR depends on observing subtle line-shape changes due to the Zeeman perturbation. In addition, this technique suffers from poor signal-to-noise ratios. High-field ^{75}As NMR provides better signal-to-noise ratios, but still requires inferring the bonding arrangements from the observed line shapes. Often these line shapes are calculated by treating the quadrupolar broadening as a perturbation on the Zeeman interaction. However, in the chalcogenide crystals and glasses, the quadrupole broadening of the ^{75}As line shape is so large that treating the quadrupolar interaction as a perturbation on the Zeeman interaction does not give an accurate description of the line shape. The error introduced by perturbation theory becomes particularly significant when one tries to compare subtle differences of the local bonding arrangements at different As sites. In this paper, we report results concerning asymmetries in the local bonding of As sites in As_xS_{1-x} and As_xSe_{1-x} glasses using high field ^{75}As NMR. We simulate the high-field ^{75}As NMR line shapes using numerical diagonalization of the full Hamiltonian in the laboratory frame, and compare the simulations with the experimental results to obtain more detailed information concerning the local order in these materials. Section II describes the simulations. The experimental methods, experimental results, and a discussion of the results are given in Secs. III, IV, and V, respectively.

The EFG produced at an As site is defined by the tensor $\overleftrightarrow{V}$, whose nine components, V_{ij} in Cartesian coordinates, can be written as[11]

$$V_{ij}=\frac{\partial^2 V}{\partial x_i \partial x_j} \quad (x_i, x_j = x,y,z), \tag{1}$$

where V is the electrostatic potential at an As site. In the principal axis system (PAS) of $\overleftrightarrow{V}$, the only nonvanishing components are V_{xx}, V_{yy}, and V_{zz}. The Laplace equation gives

$$V_{xx}+V_{yy}+V_{zz}=0. \tag{2}$$

Therefore only two independent components characterize the EFG tensor. Two commonly used parameters are the quadrupole coupling parameter q and asymmetry parameter η. They are defined as

$$\eta=\frac{|V_{xx}-V_{yy}|}{|V_{zz}|},$$

$$q=\frac{V_{zz}}{e}, \tag{3}$$

where V_{zz} is chosen such that its magnitude is the maximum of the three components. The quadrupole coupling frequency ν_Q is defined as

$$\nu_Q = \frac{3e^2qQ}{2I(2I-1)}, \tag{4}$$

where Q is the quadrupole moment of the nucleus and I is the nuclear spin. The Hamiltonian of the quadrupole interaction is

$$\mathcal{H}_Q = \frac{h\nu_Q}{6}[(3I_z^2 - I^2) + \eta(I_x^2 - I_y^2)]. \tag{5}$$

NQR of ^{75}As is performed at zero magnetic field. In this case, the eigenstates $I_z = \pm\frac{3}{2}$ and $I_z = \pm\frac{1}{2}$ are degenerate, and, therefore, only one NQR transition ($I_z = \pm\frac{3}{2} \leftrightarrow I_z = \pm\frac{1}{2}$) exists. The experimentally observed NQR frequency ν_{NQR} can be expressed as[11]

$$\nu_{NQR} = \nu_Q\left(1 + \frac{\eta^2}{3}\right)^{1/2}. \tag{6}$$

As can be seen from Eq. (6), both the coupling constant ν_Q and the asymmetry parameter η enter the equation for the single NQR transition. Therefore, these two parameters cannot be determined independently by NQR alone. Additional information can be obtained from NMR, in which an external magnetic field H_0 is applied. In this case, the degeneracy of the $I = \pm\frac{3}{2}$ and $I = \pm\frac{1}{2}$ states is lifted by H_0. This situation results in a central transition ($I_z = \frac{1}{2} \leftrightarrow -\frac{1}{2}$) and two satellite transitions ($I_z = \frac{3}{2} \leftrightarrow \frac{1}{2}$ and $I_z = -\frac{1}{2} \leftrightarrow -\frac{3}{2}$). For glassy materials, near the perturbation limit, a powder average over all possible orientations of the individual As sites yields two divergences arising from the central transition. The frequency splitting of these two divergences depends on both ν_Q and η. Therefore, NMR measurements provide an additional quantity that, when combined with Eq. (6), enables one to determine both ν_Q and η.

If $\mathcal{H}_Q$ is small compared to the Zeeman interaction, perturbation theory can be used to determine the frequency splitting of the two divergences, $\Delta\nu$. In this limit the splitting is[12]

$$\Delta\nu = \frac{\nu_Q^2[I(I+1) - (3/4)]}{144\nu_0}(\eta^2 - 22\eta + 25), \tag{7}$$

where ν_0 is the operating frequency of the spectrometer. By combining Eqs. (6) and (7), both ν_Q and η can be determined. In the cases where perturbation theory does not apply, such as in the glassy As_xS_{1-x} and As_xSe_{1-x} systems, the dependence of $\Delta\nu$ on ν_Q and η is much more complicated, and diagonalization of the full Hamiltonian is required. The procedure of constructing the powder averaged line shape is described in Sec. II.

The local order in the stoichiometric chalcogenide glasses is similar to that of their crystalline counterparts. The bonding can be described by the $8-N$ rule, according to which each As atom is threefold coordinated and each S or Se atom is twofold coordinated. For the binary systems, As_xS_{1-x} and As_xSe_{1-x}, the stoichiometry is satisfied for the compositions As_2S_3 and As_2Se_3. At these compositions there exist only As-S and As-Se bonds. In these materials, the building blocks of the random network are AsS_3 or $AsSe_3$ pyramids, in which each As atom is bonded to three S or Se atoms and each S or Se atom is bonded to two As atoms. In the arsenic-rich cases, additional bonding configurations, such as $S_2As\text{-}AsS_2$, also exist, in which some As atoms have As-As bonds. For $As_{0.5}Se_{0.5}$, if the bonding is completely determined by chemical ordering, then each As atom has exactly one As-As bond. Saleh *et al.* studied the NQR line shapes in detail for various arsenic compositions, and determined the fraction of As sites with one As-As bond, b, as a function of the normalized arsenic concentration x as follows:[8]

$$b = \frac{5x-2}{x}. \tag{8}$$

The presence of different bonding configurations can be probed by NQR, because very different NQR frequencies arise from these different As sites. The intermediate range order in these materials consists of rings and chains.

For the stoichiometric compositions, several models have been proposed. Among them is the ''raft model'' proposed by Phillips,[1] in which alternating As and S or Se atoms form a 12-membered ring structure. One consequence of this model on the local order is a large asymmetry in the electric-field gradient at some As sites. This model is supported by the Zeeman perturbed ^{75}As NQR,[9] but is in contradiction with recent experimental evidence from high-field NMR.[10]

II. SIMULATION OF THE LINE SHAPES AND DATA ANALYSIS

For amorphous materials, the sites are randomly oriented. Therefore the resonance spectrum is an average of the resonance over all possible orientations of the principal axes of the quadrupolar tensor with respect to the applied magnetic field. Such a resonance spectrum is called a powder pattern. Typically, three Euler angles (θ, ϕ, ψ) are chosen to describe the orientation, and the actual absorption line shape $S(H)$ within an interval dH about a magnetic field H can be expressed as[12]

$$S(H)dH = 4\pi\sum_m \int_H^{H+dH} I_m(\Omega)d\Omega(H_m), \tag{9}$$

where $S(H)$ is called the shape function and $d\Omega(H_m)$ is the element of solid angle such that $H < H_m < H + dH$. The function $I_m(\Omega)$ is the transition probability for a given transition. In the perturbation regime, m refers to the transition $m \rightarrow m-1$, whose probability is independent of the orientation. However, in the nonperturbation regime, m is not a good quantum number. Therefore $I_m(\Omega)$ is the transition probability for a specific transition, which depends on all three Euler angles. However, as will be shown later, it is possible to find a reduced transition probability $I_m(\theta, \phi)$ that is independent of ψ. $I_m(\theta, \phi)$ can be expressed as

$$I_m(\theta, \phi) = \frac{1}{2\pi}\int_0^{2\pi} I_m(\theta, \phi, \psi)d\psi. \tag{10}$$

For ^{75}As with nuclear spin $I = \frac{3}{2}$, the total spin Hamiltonian in a static magnetic field H_0 can be written as

$$\mathcal{H}=\mathcal{H}_Z+\mathcal{H}_Q+\mathcal{H}_S, \tag{11}$$

where $\mathcal{H}_Z$ is the Zeeman Hamiltonian, $\mathcal{H}_Q$ is the quadrupole Hamiltonian defined in Eq. (5), and $\mathcal{H}_S$ is the Hamiltonian due to magnetic shift interactions, such as the Knight shift in metallic materials, or the chemical shift in paramagnetic or diamagnetic materials. The PAS of the EFG tensor is chosen to quantize the spin operators. The orientation of the external field H_0 is defined by a set of Euler angles (θ,ϕ,ψ) with respect to the PAS. The definition of the Euler angles is consistent with that given by Goldstein.[13] In such a coordinate system, $\mathcal{H}_Z$ can be expressed as

$$\mathcal{H}_Z=-\gamma\hbar H_0(I_x\sin\theta\sin\phi-I_y\sin\theta\cos\phi+I_z\cos\theta), \tag{12}$$

where γ is the gyromagnetic ratio of ^{75}As and θ and ϕ are two of the three Euler angles defining the orientation of the static field $\vec{H}_0$ with respect to the PAS of the EFG. From Eq. (12) it can be seen that $\mathcal{H}_Z$ does not depend on the angle ψ. The magnetic shift Hamiltonian $\mathcal{H}_S$ can generally be characterized by three components K_1, K_2, and K_3 along the principal axes of the interaction tensor. The principle axes of the quadrupolar tensor are generally not coincident with those of the shift tensor. However, because of lack of knowledge of their relative orientations in powdered samples, it is usually assumed that they are coincident with each other. The verification of this assumption generally relies on a comparison between the simulation and the experimental results. Based on such an assumption, the magnetic shift Hamiltonian takes the form

$$\mathcal{H}_S=\gamma\hbar H_0(I_xK_1\sin\theta\sin\phi-I_yK_2\sin\theta\cos\phi+I_zK_3\cos\theta), \tag{13}$$

where K_1, K_2, and K_3 are the components along the x, y, and z axis in the PAS of the shift tensor $\vec{\vec{K}}$. Diagonalization of the full Hamiltonian gives the energy eigenvalues as functions of the Euler angles and the static field H_0. The transition frequencies can be obtained from the energy differences between each pair of energy levels. A random number generator is used to generate random Euler angles.

A good initial estimate of the resonant field $H^{(0)}$ can be obtained from the perturbation calculation. This value is given by[14]

$$\begin{aligned}\gamma H^{(0)}=\nu_0-\frac{1}{2}\left(m-\frac{1}{2}\right)+\nu_Q[3\cos^2\theta-1-\eta\cos 2\phi\sin^2\theta]\\ +\frac{\nu_Q^2}{12\nu_0}\left\{\frac{3}{2}\sin^2\theta[(A+B)\cos^2\theta-B]\right.\\ +\eta\cos 2\phi\sin^2\theta[(A+B)\cos^2\theta+B]+\frac{\eta^2}{6}[A-(A\\ \left.+4B)\cos^2\theta-(A+B)\cos^2 2\phi(\cos^2\theta-1)^2]\right\},\end{aligned} \tag{14}$$

where $H^{(0)}$ is the resonant field calculated to second-order perturbation in the quadrupolar and magnetic shift interactions, ν_0 is the operating frequency of the spectrometer, and the coefficients A and B are given as[14]

$$\begin{aligned}A&=24m(m-1)-4I(I+1)+9,\\ B&=\tfrac{1}{4}[6m(m-1)-2I(I+1)+3].\end{aligned} \tag{15}$$

On the other hand, it is well known that in the nonperturbative regime, multiple values of the resonant field can, in principle, exist for the same orientation of the interaction tensor. In order to take into account this effect, an additional search is performed starting at an initial value $H^{(0)}=0$ to pick up the lower resonant field. If a different value of the resonant field is found, the contribution from this transition is added to the total intensity. However, due to the lack of a rigorous estimate of where the additional resonant field might occur, this method does not always yield an additional resonant field. Nevertheless, we found that for the experimental conditions discussed in the present paper, no additional resonant fields occur. This situation will be discussed in greater detail in Appendix A.

Several methods can be used to find the resonant field with the initial estimate $H^{(0)}$ given in Eq. (14). Newton's method requires calculation of the first derivative, and, therefore, an additional diagonalization of the Hamiltonian. Also, even for a well-behaved function, this method could result in a dead loop, as discussed in many treatises on numerical methods.[15] An alternative is to use the variational methods proposed by Palangié,[16] and later employed by Abart *et al.*[17] The full Hamiltonian can be expressed as

$$\mathcal{H}=H^{(0)}\hat{\mathcal{G}}+\mathcal{H}_Q, \tag{16}$$

where $\hat{\mathcal{G}}$ is a field-independent operator. For a given trial field $H^{(0)}$, a better estimate of the field $H^{(1)}=H^{(0)}+\delta H$ can be obtained from[17]

$$\delta H=\frac{\hbar\omega_0-\hbar[|\omega_i(H^{(1)})-\omega_j(H^{(1)})|]}{\langle i|\hat{\mathcal{G}}|i\rangle-\langle j|\hat{\mathcal{G}}|j\rangle}, \tag{17}$$

where $\hbar\omega_i$ is the energy of the ith energy level. The new field $H^{(1)}$ is then used to construct a new Hamiltonian. This procedure is repeated until the differences between the operating frequencies and the transition frequencies, as obtained from the differences of the eigenvalues, are smaller than a predefined value ϵ. This method does not require an additional diagonalization, and, therefore, it can reduce computing time significantly.

In the nonperturbation regime, some transitions that are forbidden by the selection rules become allowed. Therefore, transitions between each pair of energy levels are considered, regardless of the condition $\Delta m=\pm 1$. For the same reason, the transition probability is instead calculated according to

$$P\propto|\langle f|\mathcal{H}_1|i\rangle|^2, \tag{18}$$

where $\mathcal{H}_1$ is the Hamiltonian due to the applied oscillating field in the plane perpendicular to $\boldsymbol{H}_0$, $|f\rangle$ is the final state, and $|i\rangle$ is the initial state. Assuming that the amplitude of the oscillating field, $\boldsymbol{H}_1$, is along the x axis in the laboratory frame, $\mathcal{H}_1$ can be written in the PAS as

$$\mathcal{H}_1 = -\gamma\hbar H_1[I_x(\cos\psi\cos\phi - \cos\theta\sin\phi\sin\psi) + I_y(\cos\psi\sin\phi + \cos\theta\cos\phi\sin\psi) + I_z\sin\theta\sin\psi]. \tag{19}$$

P can be calculated by combining Eqs. (18) and (19).

Obviously, when searching for forbidden transitions that might contribute to an additional resonance at lower field, it is likely that no resonant field exists, and the program may get into a dead loop. To avoid this, an internal counter monitors the iterations. If no resonant field is found after ten iterations, an internal flag will be set. At this point the program will skip the point, save the values of the Euler angles and the trial field in a log file, and continue the simulation. The energy-field relation at those angles can later be reproduced by numerically solving the secular equation, and this relation can be compared to the simulation. This procedure discriminates between the possibility that there is no resonant field at these given angles for a certain transition, and the possibility that the iteration does not converge even though there exists a resonant field. In fact, extensive tests of the program show that, for an initial value given by Eq. (14), the resonant field can be found after only two to three iterations if there exists a resonant field.

For glassy samples, there is significant broadening of the NQR line shapes due to the distributions of both ν_Q and η. However, as can be seen from Eq. (6), for small variations of η, the variation of the NQR frequency is also small, typically less than a few percent. Typical NQR line shapes in these glassy samples have widths that are about 10% of the central frequency. Therefore, the first assumption is that the broadening due to variations in η is not important in determining the NQR line shape. In this case, the distribution of η can be assumed to be independent of ν_Q. For simplicity a Gaussian function is assumed for the distribution of η,

$$f(\eta) = \frac{1}{\sqrt{2\pi}\sigma_\eta} e^{-(\eta-\eta_0)^2/2\sigma_\eta^2}, \tag{20}$$

where η_0 is the average value of the distribution and σ_η is the standard deviation of the distribution in the asymmetry parameter.

To obtain both ν_Q and η, the NQR line shape is first fitted to obtain the distribution of ν_{NQR}. A series of NMR line shapes is simulated with different values of ν_{NQR}, each with a distribution of η. These normalized lines are then summed using the distribution of ν_{NQR} as the weighting factors. The values of η_0 and σ_η are then varied to fit the NMR line shape. In this way, both the NQR and the NMR line shapes are consistently fitted. Due to the constraints imposed by the NQR line shape, the only adjustable parameters in fitting the NMR line shape are η_0 and σ_η. Again, for simplicity, the NQR line shapes are fitted with a Gaussian function

$$f(\nu) = \frac{1}{\sqrt{2\pi}\sigma} e^{-(\nu-\nu_0)^2/2\sigma^2}, \tag{21}$$

where ν_0 is the central NQR frequency and σ_Q is the standard deviation of the frequency distribution. However, in the cases where multiple As sites exist, the NQR lineshape may consist of contributions from different bonding configurations. In this case, the NQR line shape is decomposed into several Gaussian functions for each type of bonding configuration, and different values of η_0 and σ_η are used for each type of bonding configuration.

III. EXPERIMENTAL METHODS

In the chalcogenide crystals and glasses discussed in this paper, the broad line shapes of the ^{75}As NMR, which are about 10 T broad at a central field of about 17 T, make it impossible to use conventional pulsed-NMR techniques. The line shapes are constructed by scanning the magnetic field in small steps, with a fixed operating frequency. At each value of the field, a 90°-180° pulse sequence is used to produce an echo. The echo height is proportional to the area under the resonance line shape within an interval of the field that is determined by the RF pulse width. If the pulse sequence is kept the same during the measurements, then the plot of echo height as a function of magnetic field will be the same as the resonance line shape. This procedure assumes that there is negligible variation of the spin-spin relaxation time T_2 across the line shape. The advantage of this technique is that it utilizes the higher signal-to-noise ratio of pulsed NMR to probe the entire broad line shape.

Several samples with different glass compositions have been measured, including glassy As_2S_3, As_2Se_3, and $As_{0.5}Se_{0.5}$. For comparison, polycrystalline As_2S_3 and As_2Se_3 were also measured. Because of the difficulty in synthesizing crystalline As_2S_3, a natural mineral (orpiment) sample was employed. The line shape of *a*-As was also measured for comparison.

The NMR measurements were performed on 24.6-T and 35-T resistive magnets at the National High Magnetic Field Laboratory (NHMFL), using a conventional pulsed-NMR spectrometer from Tecmag. The samples were cooled in liquid nitrogen, to increase the signal-to-noise ratio. A typical 90° pulse width was about 2 μs. The resolution of the field was limited by the dc current controller of the magnet. The minimum step size for changing the magnetic field was about 150 G.

IV. EXPERIMENTAL RESULTS

A. Polycrystalline As_2S_3 and As_2Se_3

Polycrystalline As_2S_3 and As_2Se_3 provide a good starting point for understanding the bonding configurations of the chalcogenide glasses. In crystalline As_2S_3 and As_2Se_3, there exist two inequivalent arsenic sites,[5] with different bond angles and slightly different bond lengths. The slight difference in bond angles and lengths results in different values of ν_Q and η. The widths of the NQR line shapes for these samples are about 100 to 200 kHz, which do not significantly broaden the NMR line shape. Therefore, for the purpose of calculating the NMR line shapes, the distributions of NQR frequencies can be assumed to be δ functions.

Figure 1 shows the NMR line shape for polycrystalline As_2Se_3 at 77 K and an operating frequency ν_0

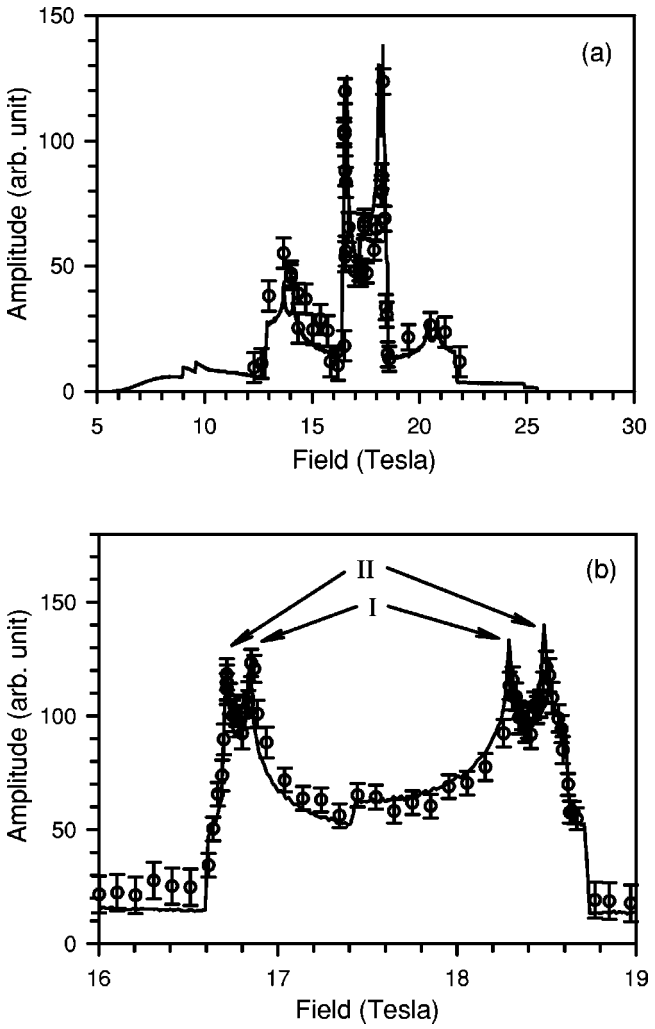

FIG. 1. ^{75}As NMR line shape of polycrystalline As_2Se_3 at 77 K. The open circles and the solid lines represent the data and the fit, respectively. (a) Full line shape at $\nu_0 = 125.57$ MHz. (b) Resolved line shape of the central transition at $\nu_0 = 127.06$ MHz. The two inequivalent As sites are denoted by I and II. The values of η for these two inequivalent As sites are $\eta = 0.17$ for $\nu_Q = 55.80$ MHz (site I) and $\eta = 0.11$ for $\nu_Q = 60.13$ MHz (site II), respectively.

$= 127.06$ MHz. These data were first reported in Ref. 10. Figure 1(a) shows the full line shape. Figure 1(b) shows the resolved structure in the central transition on an expanded scale. The data are fitted using the two NQR frequencies reported previously.[18] Figure 1(b) clearly shows two distinct As sites, with different values of ν_Q and η. The values of η are 0.11 ± 0.01 for $\nu_Q = 60.13$ MHz and 0.17 ± 0.01 for $\nu_Q = 55.80$ MHz.

The NMR line shape and the fit to the central transition in polycrystalline As_2S_3 are shown in Fig. 2.[10] The two NQR frequencies at 77 K are also taken from previously reported results.[19] In Fig. 2, there is a significant discrepancy between the fit and the data near the high-field divergence. There are two possible reasons for this discrepancy. The first is an inaccurate measurement of the line shape. Because of the narrow widths of the divergences in the crystal, it is difficult experimentally to define the line shape in the vicinity of the

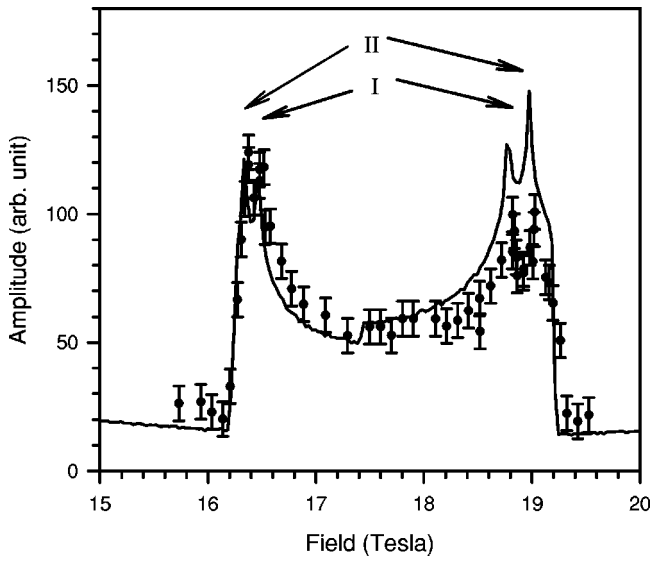

FIG. 2. The resolved ^{75}As NMR line shape of the central transition at 77 K for polycrystalline As_2S_3. The operating frequency is $\nu_0 = 127.06$ MHz. The solid circles and the solid line represent the data and the fit, respectively. The values of η for the two inequivalent As sites are $\eta = 0.15$ for $\nu_Q = 70.12$ MHz (site I) and $\eta = 0.08$ for $\nu_Q = 72.70$ MHz (site II), respectively.

divergence. Since the sample is from a natural crystal, the second possible reason for the discrepancy is that the As_2S_3 crystal is strained. This reason is consistent with a report that the NQR line shape is somewhat distorted.[5] In any case, the fit to the line shape is still in reasonably good agreement with the data. The values of η and ν_Q for this sample are $\eta = 0.15$, $\sigma_\eta = 0.02$ for $\nu_Q = 70.12$ MHz and $\eta = 0.08$, $\sigma_\eta = 0.02$ for $\nu_Q = 72.70$ MHz.

For both polycrystalline samples, the values of η are less that 0.2. These small values of η suggest that in these crystalline materials, the EFG is very close to axially symmetric. This result is consistent with the fact that the apex pyramidal bond angles for the three As-S or As-Se bonds are nearly the same.

B. Glassy As_xSe_{1-x} binary system

Figure 3 shows the previously published NQR line shape of As_2Se_3,[8] and Fig. 4 shows the corresponding NMR line shape. Both spectra were obtained at 77 K. In Fig. 3, the NQR frequencies of the corresponding crystal are shown at the bottom as vertical dashed lines. It can be seen that although the line shape is significantly broader than in the crystal, the magnitude of the quadrupolar coupling, as reflected by the center of the NQR line shape, is very close to that in the crystals. The line shape is fitted according to Eq. (21). The central NQR frequency is 57.9 MHz, with a width $\sigma \approx 2.9$ MHz. The NMR line shape is fitted by assuming a distribution of η according to Eq. (20). Figure 4 shows the data and the fit to the NMR line shape. The value of η_0 is 0.18 as compared to 0.11 and 0.17 in the crystal, and the width is $\sigma_\eta = 0.1$. Indeed, the variation of η is small. This small variation provides an *a posteriori* justification for the assumption made in Sec. II that the broadening of the NQR

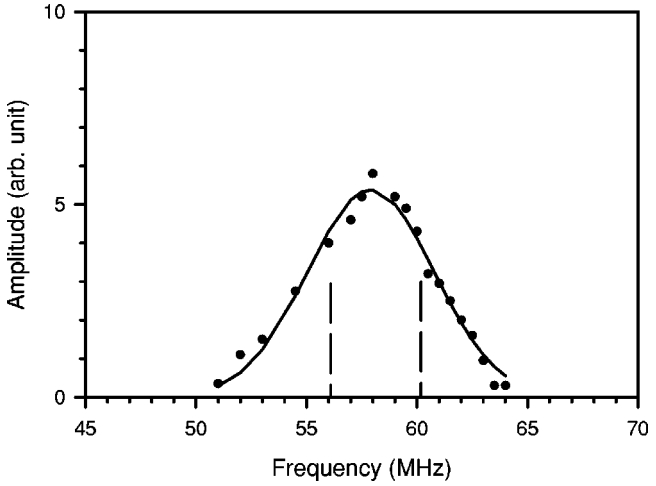

FIG. 3. The NQR line shape of glassy As_2Se_3. The solid circles and the solid line represent the data and the fit, respectively. The vertical dashed lines represent the NQR frequencies in the crystal (56.07 MHz and 60.25 MHz). The data are fitted with a Gaussian function. The central frequency of the fit is 57.9 MHz, and the width of the fit is $\sigma_Q \approx 2.86$ MHz.

line shape is predominantly due to the variation of ν_Q.

Figure 5 shows the NQR line shape for glassy $As_{0.5}Se_{0.5}$ at 77 K. The NQR frequencies for both crystalline As_2Se_3 and crystalline As_4Se_4 are shown as vertical lines at the top of the figure. For crystalline As_4Se_4, which has the same composition as $As_{0.5}Se_{0.5}$, each As atom has one As-As bond. As a result of this bonding arrangement, the NQR frequencies in this crystal are much higher than those in crystalline As_2Se_3.[20] These NQR frequencies in the crystals enable us to identify the different arsenic sites in the glass. As mentioned in Sec. I, in glassy $As_{0.5}Se_{0.5}$, if the bonding is determined completely by chemical ordering, then each arsenic site has one As-As bond. However, it is clear from Fig. 5 that the bonding cannot be described by complete chemical ordering. In addition to the dominant peak at about 80 MHz, which has an NQR frequency similar to those in crystalline As_4Se_4, there is a tail to lower frequency, which extends to about 60 MHz. The smaller peak at the lower frequency is suggestive of the presence of arsenic sites with no As-As bonds. This attribution is made by comparison with the NQR frequencies in the corresponding As_2Se_3 crystal. Clearly, some statistical fluctuations exist in the bonding configurations that occur in the glass. In order to maintain the correct composition of the glass, there should exist As sites with two As-As bonds, whenever there are As sites with no As-As bonds. For this reason, we decompose the line shape into three Gaussian functions, as denoted by *A*, *B*, and *C* in Fig. 5. By comparison with the NQR frequencies in crystals, we can identify curve *A* as the signal due to As atoms bonded to three Se atoms, i.e., with no As-As bond, and curve *C* as due to As atoms with one As-Se bond. Previously reported values of ν_{NQR} for As sites in molecular crystals, such as As_3Se_4, in which each As site contains two As-As bonds, do not show NQR frequencies in the range denoted by curve *B*. However, these crystalline structures probably have very different bond angles than those occurring in glassy materials, because they

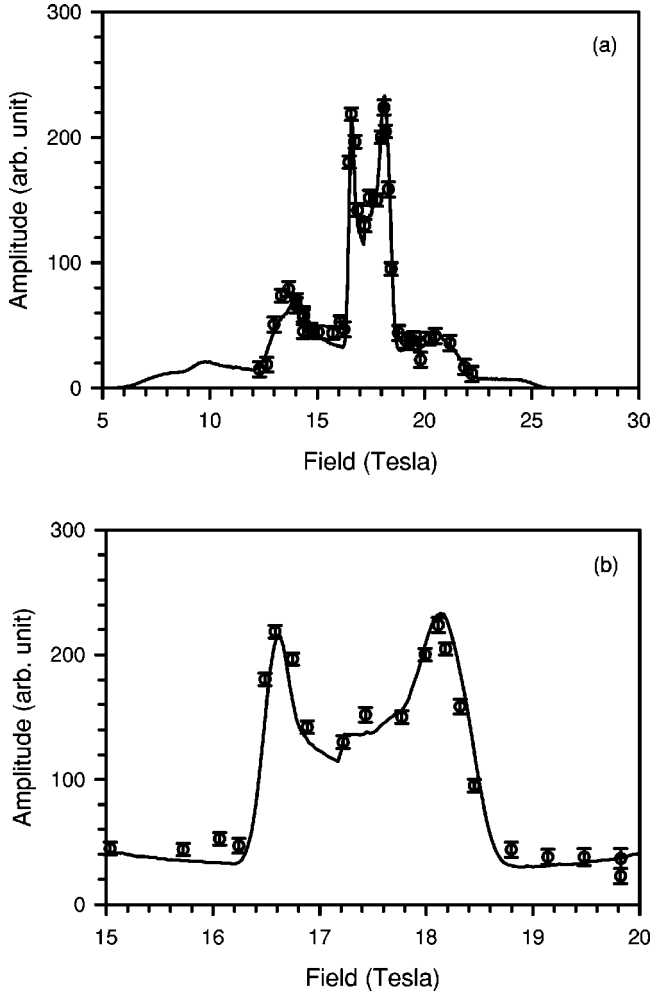

FIG. 4. ^{75}As NMR line shape of glassy As_2Se_3 at 77 K. The operating frequency is $\nu_0 = 125.57$ MHz. The solid circles and the solid lines represent the data and the fit, respectively. (a) Full line shape. (b) Central transition on an expanded scale. The parameters for the distribution of η are $\eta_0 = 0.18$ and $\sigma_\eta = 0.1$.

contain three-membered As rings. Therefore in order to preserve both the stoichiometry and the chemical order (i.e., three-fold coordinated As and two-fold coordinated Se) we assume that curve *B* corresponds to As sites, which have two As-As bonds and one As-Se bond.

The NMR line shape and the fit are shown in Fig. 6, where the values of η for each type of As site have been independently adjusted to fit the experimental data. The values of η_0 are $\eta_0 \approx 0.16$ for curves *A* and *B*, which represent As sites with zero and two As-As bonds, respectively. The value of η_0 is $\eta_0 \approx 0.6$ for curve *C*. Apparently, the presence of one As-As bond at an As site results in a much larger value of the asymmetry parameter ($\eta_0 \approx 0.6$), presumably due to the different electronegativities of the As and Se atoms. Because of the lack of resolved structure, particularly in the NQR spectrum of Fig. 5, the fits to the NQR and NMR spectra are not unique. Our philosophy, therefore, must be to capture the essence of the microscopic model for the As sites with the smallest number of adjustable parameters. For this reason, we ignore any distributions in the asymmetry param-

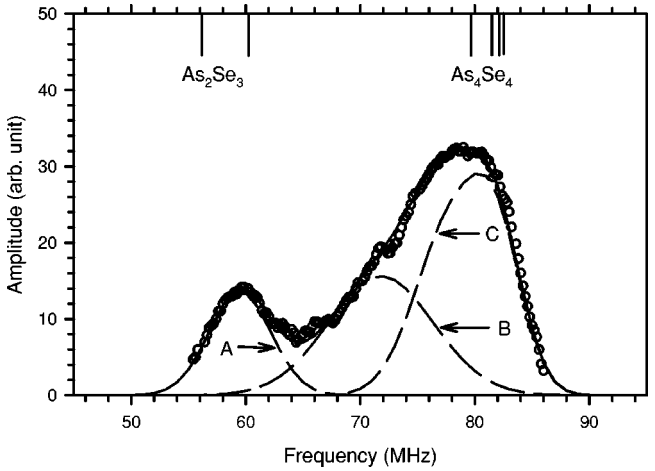

FIG. 5. NQR line shape of glassy $As_{0.5}Se_{0.5}$ at 77 K. Open circles represent data. The dashed lines represent the decomposition of the line shape. The NQR frequencies in crystalline As_2Se_3 and As_4Se_4 are shown as solid vertical lines at the top. The dashed curves *A*, *B*, and *C* are decomposed line shapes for the arsenic sites with zero, two, and one As-As bonds, respectively. The solid line is the sum of curves *A*, *B*, and *C*.

eter η for the three types of sites, even though variations certainly exist in the real glass. Note that in Fig. 6(b), the small bump near 14 T is due to the approximation of a unique value of η, as are probably the three peaks in the lower-field region of Fig. 6(a). These features can be smoothed out by assuming a distribution of η. For the arsenic sites with no As-As bonds, the value of $\eta \approx 0.16$ is very close to that in stoichiometric glassy As_2Se_3. Also, η is much larger for the As sites with one As-As bond. This difference enables us to clearly distinguish the two different local bonding configurations, i.e., the sites with one As-As bond and the sites with no As-As bonds. In addition, the arsenic sites with two As-As bonds have a value of η that is similar to those with no As-As bonds. This empirical result is rather surprising and not understood.

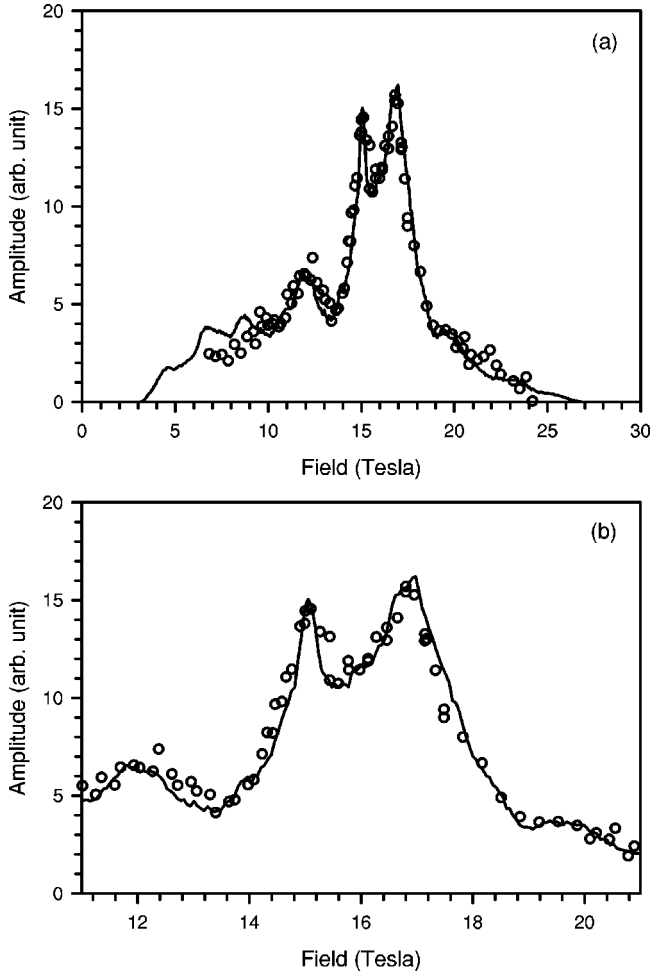

FIG. 6. ^{75}As NMR line shape of glassy $As_{0.5}Se_{0.5}$ at $\nu_0 = 115.21$ MHz. The open circles and the solid line represent the data and the fit, respectively. (a) Full line shape. (b) Central transition on an expanded scale. The values of η_0 are $\eta_0 = 0.16$ for curves *A* and *B* in Fig. 5 (As sites with zero or two As-As bonds, respectively), $\eta_0 = 0.6$ for curve *C* in Fig. 5 (As sites with one As-As bond).

C. Glassy As_xS_{1-x} binary system

Figure 7 shows the NQR line shape of glassy As_2S_3 at $T = 77$ K. Except for the long tail extending to higher frequencies, this line shape is very similar to that for glassy As_2Se_3 shown in Fig. 3. The major difference is the higher frequency, which is probably a result of the larger electronegativity difference between As and S. Compared to the NQR line shape of glassy $As_{0.5}Se_{0.5}$, the majority of the As atoms in glassy As_2S_3 do not have As-As bonds. However, unlike glassy As_2Se_3, this particular sample of glassy As_2S_3 does have some As-As bonds as indicated by the low-intensity tail extending up to about 90 MHz. Presumably, this feature is due to a slight departure from stoichiometry. The frequencies in crystalline As_2S_3 and As_4S_4 are shown in the figure as vertical solid lines.[19,21] The major peak is fitted with a Gaussian function with center at ~ 72 MHz with a width $\sigma \sim 3$ MHz. This peak can be identified as due to the As sites bonded to three sulfur atoms, i.e., with no As-As bonds. By subtracting this component from the experimental data, it is found that the high-frequency tail may have two components, as shown in the inset in Fig. 7. The small peak centered near 90 MHz probably is due to As atoms with one As-As bond. This attribution is made by comparison with the NQR frequencies in crystalline As_4S_4, where each arsenic atom has one As-As bond. The identification of the small peak near 82 MHz, if indeed it exists, is probably due to As sites with two As-As bonds.

The fit to the NMR line shape at 127.05 MHz for this sample is shown in Fig. 8. This fit, which accurately reproduces the NMR spectrum, assumes three types of As bonding sites. Figure 8(a) shows the full spectrum. Figure 8(b) shows the central transition on an expanded scale. By analogy with the fit to the NMR spectrum for glassy As_2Se_3 (Fig. 4), the vast majority of the As sites have no As-As bonds, and $\eta_0 = 0.16$ for these sites. The width of the distribution of η is $\sigma_\eta = 0.03$. For the sites with one As-As bond, $\eta = 0.6$. The

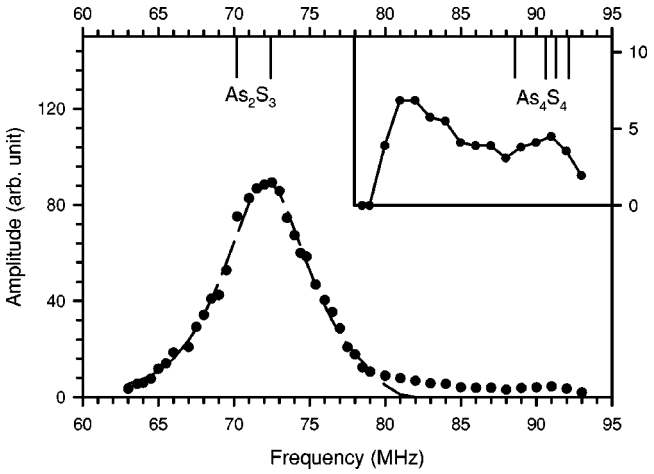

FIG. 7. NQR line shape of glassy As_2S_3 at $T=77$ K. The solid circles represent experimental data. The vertical solid lines represent the corresponding NQR frequencies in As_2S_3 and As_4S_4 crystals, as labeled. The dashed line is a fit to the main peak using a Gaussian function. The inset shows the portion of the line shape at higher frequencies, on an expanded scale, after subtracting the fit from the data.

third contribution, whose origin is unknown but may be due to As sites with two As-As bonds, was fitted for simplicity with the same η_0 and σ_η as the primary sites.

Figure 9 shows a second NMR line shape at a slightly different operating frequency at 125.69 MHz. The spectrum contains data at lower magnetic fields. It can be seen from Fig. 9(a) that the fit agrees with the data very well even down to the lower fields. Figure 9(b) shows the fit to the central portion of the spectrum on an expanded scale. The parameters are the same as those used to fit Fig. 8. These results are consistent with the assumption made in Sec. II that although different As sites occur, broad distributions of η for these sites are not present in these materials.

The asymmetry parameters and their distributions for the three different bonding configurations are summarized in Table I. It can be seen from Table I that the asymmetry parameters for different bonding configurations are consistent among the various glass compositions studied.

D. Amorphous arsenic

The NMR and NQR line shapes of amorphous arsenic have also been studied. In this amorphous solid, both the NQR and NMR line shapes are much more sensitive to distortions in the arsenic pyramidal sites because there are no twofold coordinated ''bridges'' to relax the strains in the random network. Every arsenic site is bonded to three other arsenic sites so that any bond angle fluctuations directly affect the pyramidal apex angles. The NQR line shape in amorphous arsenic has been studied previously,[7,22] and here we compare it with the high-field NMR line shape. Figure 10 shows the NQR line shape at 4.2 K.[7,22] The solid line is the smooth curve that we assume represents the NQR line shape to be used in fitting the NMR line shapes self-consistently. This line shape remains the same up to 77 K, and therefore, can be compared with the NMR line shape at 77 K. Figure 11

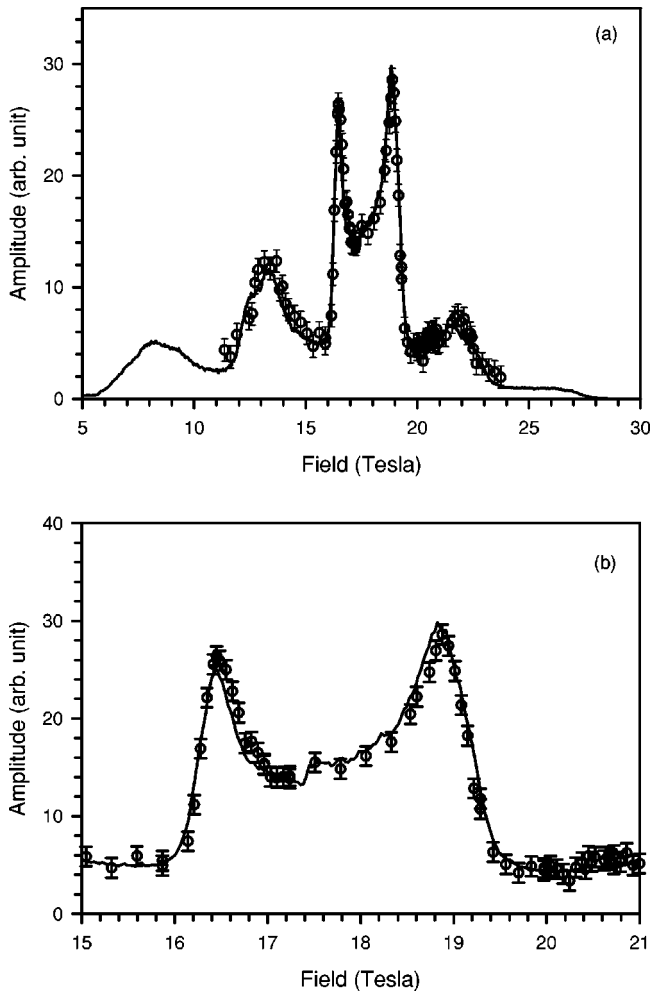

FIG. 8. ^{75}As NMR line shape of glassy As_2S_3 at $T=77$ K. The open squares and the solid lines represent the data and the fit, respectively. (a) Full line shape. (b) Central transition on an expanded scale. The values of η are $\eta=0.14$ for As sites with no As-As bonds and for the central region of the NQR spectrum. The value of $\eta=0.6$ for As sites with one As-As bond.

shows the NMR line shape at 77 K and the fit corresponding to the solid line in Fig. 10 with the distribution of ν_Q and η discussed below. The tail extending to lower frequency makes it impossible to fit the NQR line shape with a Gaussian function, and there is no physical justification for decomposing this line shape into several Gaussian functions. In principle, one may be able to assume a specific form of distribution for both ν_Q and η, and self-consistently convolute these two distributions to reproduce the NQR line shape. However, in the absence of a detailed structural model for amorphous arsenic, it is not possible to find unique distributions in ν_Q and η. Therefore we simulated the NQR line shape by assuming a Gaussian function for the distribution of η, while Eq. (6) is employed to ensure that each value of η reproduces the NQR line shape of Fig. 10 independently. In order to fit the NMR spectrum of Fig. 11, it is necessary to assume a much broader distribution of η than is required to fit the spectra for the binary systems. In the Gaussian function, the ''average'' value of η is 0.6 and the width of the

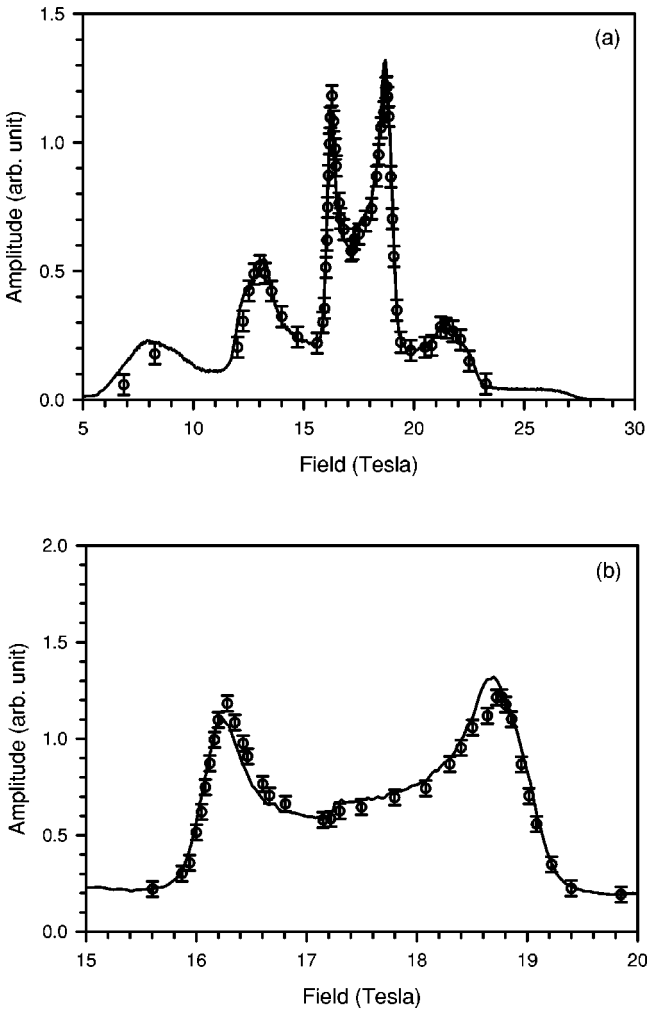

FIG. 9. ^{75}As NMR line shape of glassy As_2S_3 at $T=77$ K. The operating frequency is 125.69 MHz. The open circles and solid lines represent the data and the fit, respectively. (a) Full line shape. (b) Central transition on an expanded scale. The values of η are $\eta=0.14$ for As sites with no As-As bonds, and for the central region of the NQR spectrum. The value of η is 0.6 for the As sites with one As-As bond.

distribution is 0.4, but the distribution extends only over the allowed values of η $(0\leqslant\eta\leqslant1)$ It has been suggested that the asymmetry in the NQR line shape is due to the distribution of the dihedral angles in this material.[7,22] However, the results from these previous calculations[7,22] do not reproduce the NQR line shape very accurately. In particular, the asymmetry at the low frequency is not as pronounced as in the experimental spectrum. Further progress awaits the availability of a direct comparison with a detailed structural model for amorphous arsenic.

TABLE I. Summary of the asymmetry parameters for different As bonding configurations.

Bonding	As_2Se_3		$As_{0.5}Se_{0.5}$		As_2S_3	
configuration	η_0	σ_η	η_0	σ_η	η_0	σ_η
No As-As bond	0.18	0.1	0.16		$\sim$ 0.16	0.03
1 As-As bond			0.6		0.6	
2 As-As bond			0.16		0.16	

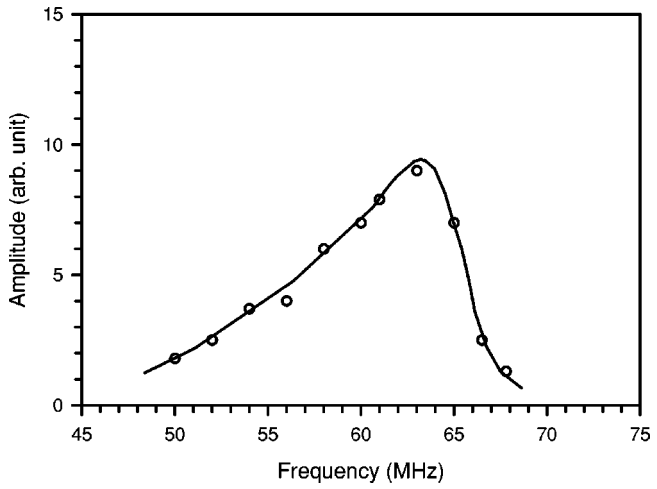

FIG. 10. The NQR line shape of *a*-As at 4.2 K. The solid circles represent data. The solid line is an aid to the eye. (Reproduced from Ref. 22 with permission.)

The small narrow peak near the central field in Fig. 11 is probably due to a small fraction of the crystalline phase incorporated in the amorphous network. The NQR frequency for rhombehedral arsenic is 22 MHz,[22] which results in a much smaller splitting between the two divergences in the NMR spectrum and probably cannot be resolved.

V. DISCUSSION

The NMR powder pattern line shapes shown in Figs. 1, 2, 4, 6, 8, 9, and 11 are calculated by the exact diagonalization of the Hamiltonian, which contains the Zeeman, chemical shift, and quadrupolar terms. As expected, in the regime where perturbation theory is appropriate, the results agree with those calculated using perturbation theory. However, when perturbation theory is not strictly valid, there are significant differences between these two approaches. Details are described in the Appendix.

Although the chemical shift interaction is included in the Hamiltonian, its influence is negligible for the ^{75}As high-field NMR data presented in this paper. Typical chemical shifts for ^{75}As, as estimated from inorganic arsenic compounds, are on the order of 10^{-3} of the Zeeman field.[23] This magnitude is too small to be measured accurately in the Bitter magnets employed for this study.

Many polymeric glasses are well described by the random network model, which assumes that there are well-defined structural units, such as the SiO_4 tetrahedra in SiO_2 glass, which are connected in a random fashion through a rather large variation in the bond angles of an element with low nearest-neighbor coordination number. In SiO_2 glass this later role is played by the two-fold-coordinated oxygen atoms. A consequence of this structure is that the SiO_4 tetrahedra remain relatively undistorted. In the chalcogenide glasses discussed here, the role of oxygen is played by sulfur or selenium, and as a consequence the AsS_3 and $AsSe_3$ py-

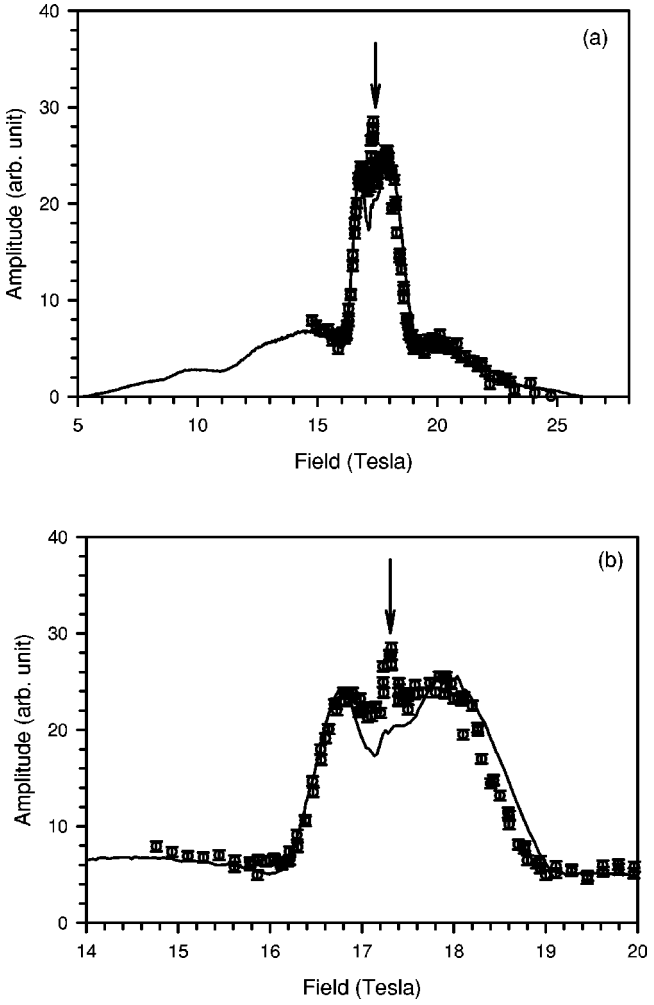

FIG. 11. NMR line shape of *a*-As at 77 K. The operating frequency is 125.69 MHz. The open circles and solid lines represent the data and the fits, respectively. (a) The full spectrum. (b) The central transition on an expanded scale. The small peak denoted by the arrow is due to a small concentration of ($<1\%$) the crystalline phase in the sample. The parameters for the distribution of η are $\eta_0=0.65$ and $\sigma_\eta=0.5$.

ramidal units remain relatively undistorted for arsenic concentrations less than or equal to the stoichiometric compositions, $As_{0.4}S_{0.6}$ and $As_{0.4}Se_{0.6}$.

For arsenic concentrations greater than $x=0.4$, two effects occur. First, the presence of like-atom (As-As) bonds has a strong influence on the asymmetry of the pyramidal units. This influence shows up in the high-field NMR as both an increase in the asymmetry parameter and as an increase in the quadrupolar coupling constant, presumably due to differences in electronegativity between the As-S or As-Se and the As-As bonds. In addition, as the arsenic concentration increases above $x=0.4$, the connectivity of the As pyramidal units becomes more and more constrained. In *a*-As, there is no ''weak chalcogen link'' that connects the arsenic atoms, and each As pyramidal site is directly affected by distortions at neighboring As sites. As we shall see below, this complication makes both the interpretation of the ^{75}As NMR spectra and the modeling of the structure much more difficult.

One other important consequence of increasing the arsenic concentration above $x=0.4$ is the fact that, in a mean-field sense, the network becomes ''rigid'' at this concentration.[24] This rigidity transition occurs when the number of degrees of freedom per atom is equal to the average number of constraints per atom. Because there can be regions that are overconstrained coexisting with regions that are underconstrained, the mean-field approach is not strictly accurate,[24] but the concept of a transition region where the rigidity percolates through the network remains. Increasing the As concentration in the As-S and As-Se glasses allows one to move continuously through the region from an underconstrained to an overconstrained network. Unfortunately, except for an increase in the inhomogeneous NMR linewidths, the present ^{75}As high-field NMR data provide no obvious test of this expected behavior.

A. Local bonding asymmetries in polycrystalline and glassy As_xS_{1-x} and As_xSe_{1-x}

For crystalline As_2S_3 and As_2Se_3, the asymmetry parameters are small, as expected from the local structure. The three bond angles between the As-S or As-Se bonds are close to each other, so the EFG's at As sites are nearly axially symmetric. For glassy As_2S_3 and As_2Se_3, despite the significant quadrupole broadening, the values of the asymmetry parameter are not significantly different from those in the crystals. Moreover, for glassy As_2S_3, even the distribution of η is small, suggesting that the majority of the AsS_3 pyramids remain almost undistorted from those in the crystal. The twofold-coordinated S or Se atoms provide enough freedom for connecting the randomly oriented pyramids without distorting each pyramid. In arsenic-rich samples ($As_{0.5}Se_{0.5}$), most of the As sites have one As-As bond for each atom, resulting in a much higher asymmetry parameter. However, since As_2Se_3 has an average coordination number of 2.4, any arsenic-rich glass will be overconstrained. For this reason, it is not easy to determine the local order at As sites, because the asymmetry parameter can be affected by both the heteronuclear As-Se or As-S bonding and the distortion of the bond angles. As seen in Fig. 6, although the overall line shape is fitted well, there are still discrepancies between the data and the fit. The effect of an overconstrained random network is further demonstrated in the case of amorphous As, in which all As atoms are threefold coordinated, and the entire network has a higher average coordination number. The very broad distribution of η is a direct result of the large distortion of the As-As bond angles. In principle, one may improve the fitting by assuming more complicated forms of the distributions of both ν_Q and η, and self-consistently convolute these two functions to fit both the NQR and the NMR line shapes, but the underlining microscopic details will still be difficult to discern.

Although no information on intermediate range order can be inferred directly from the high-field NMR measurements, these results do impose restrictions on possible models of the structure. First, the widths of the NQR (Refs. 5,8, and 25) and NMR peaks can be related to the As apex bond angle variations. In glassy $As_{0.4}S_{0.6}$ and $As_{0.4}Se_{0.6}$ one estimate of

these variations can be obtained by comparing the average apex bond angles for the two arsenic sites in the crystalline unit cells. As seen in Figs. 3 and 5, these two sites are spread apart by approximately the full width of the NQR line in the respective glasses. In the two crystalline compounds the two inequivalent arsenic sites have average apex bond angles that differ by a few degrees $(2°-5°)$, so one may infer that in the two stoichiometric glasses, the average deviations in apex bond angles are similar. If one tries to extend this very simple analysis to the $As_{0.5}Ae_{0.5}$ glass composition, the deviations become larger, but the analysis is greatly complicated by the presence of As-As bonds, which make the field gradients depart strongly from axial symmetry. A second estimate of the apex bond angle distributions can be made using a simple tight-binding model to calculate the field gradients,[5,8] and this method also yields deviations of a few degrees.

Second, the low values of η for glassy $As_{0.4}S_{0.6}$ and $As_{0.4}Se_{0.6}$ are inconsistent with at least one model[1] that has been proposed to explain the intermediate range order in these two glasses. In this model, one-third of the arsenic sites are highly distorted and should therefore have a large value of η. Sites with $\eta \approx 0.3$ were inferred from previous Zeeman perturbed NQR measurements,[9,26] but this inference required fitting subtle features in the NQR line shapes. On the other hand, the present high-field NMR results show conclusively that there are very few, if any, arsenic sites with large values of η. From the fits shown in Figs. 8 and 9, we estimate that the fraction of As sites with η greater than about 0.2 is less than about 1%.

B. Statistical influences on the bonding

During the formation of binary glasses, the structure will be influenced by both chemical ordering and statistical fluctuations. If the glass forming process is completely determined by chemical ordering, then heteronuclear bonding is preferred, while a process controlled completely by random statistics will show no preference of bonding, i.e., the numbers of heteronuclear bonds and homonuclear bonds will only depend on the composition and the number of valence electrons on each type of atom. From the experimental results on glassy $As_{0.5}Se_{0.5}$, it is easily seen that both chemical ordering and statistics are involved in the glass forming process. In particular, for systems at stoichiometry, such as As_2S_3 and As_2Se_3, the bonding is dominated by chemical ordering. In the case of glassy As_2Se_3 the NQR and NMR spectra shown in Figs. 3 and 4, respectively, are consistent with the presence of only As-Se bonds. On the other hand, for the particular sample of glassy As_2S_3 employed in this study, there is evidence from the NQR spectrum (and more subtly from the NMR spectra in Fig. 8) for the presence of As sites with one or perhaps two As-As bonds. This behavior is probably not due to any departure from chemical ordering but rather to a small departure from stoichiometry. It is well known that the As-S system is more difficult to make exactly on stoichiometry because of the high vapor pressure of sulfur. If the sample is indeed slightly As rich, then As-As bonds will naturally be formed according to the predictions of Eq. (8). From the NQR spectrum of Fig. 7 we estimate that the fraction of As sites (with NQR frequencies near 90 MHz) with one As-As bond is $\approx 3\%$. This concentration and Eq. (8) yield a value of $b = 0.402$, which means that the sample is only about 0.5% off stoichiometry.

TABLE II. Comparison with experimental results for the signal fractions from a binomial distribution and for chemical ordering in glassy $As_{0.5}Se_{0.5}$.

Bonding configuration	Binomial distribution	Chemical ordering	Experiment result
0 As-As	0.3	0	0.17
1 As-As	0.44	1	0.50
2 As-As	0.22	0	0.33
3 As-As	0.04	0	?

There are two possible interpretations for the intensity in Fig. 7 between the peaks near 72 and 90 MHz. First, this intensity may be due to distorted sites with no As-As bonds or one As-As bond or, second, due to the presence of a small number of sites with two As-As bonds. The suggestion of the presence of sites with two As-As bonds is based on an NQR study of glassy As_3Se_2, where a peak near 70 MHz has been attributed to As sites with two As-As bonds.[27] In the As-S system, this frequency would be ≈ 87 MHz. At present the data are insufficient to distinguish between these two possibilities.

If, on the other hand, the bonding is not determined by chemical ordering but is completely random, then an estimate of the fractions for the different bonding configurations can be obtained from a binomial distribution.[28] This situation may hold for As-rich compositions in the As_xSe_{1-x} $(x > 0.4)$ system. Table II compares the results from a binomial distribution and the decomposition as described in Sec. IV B for glassy $As_{0.5}Se_{0.5}$. This table also presents the results expected from perfect chemical ordering for comparison. From Table II we see that the experimental result falls somewhere in between perfect chemical ordering and a statistical distribution. This result suggests that in glassy $As_{0.5}Se_{0.5}$ the bonding configuration depends on both chemical ordering and statistical fluctuations. For the case of three As-As bonds, the NQR frequency is 60 MHz, which overlaps the region with no As-As bonds. In any case, the contribution due to these sites is expected to be small.

VI. SUMMARY

The high-field NMR, line shape can be studied in great detail using simulations of the high-field ^{75}As NMR line shape by numerically diagonalizing the full Hamiltonian in the laboratory frame. For samples that are stoichiometric $(As_{0.4}S_{0.6}$ and $As_{0.4}Se_{0.6})$, the asymmetry parameters of the electrical-field gradient at the As sites are less than 0.2 in both glassy and polycrystalline samples. The similarities between the NMR spectra in the glasses and crystals can be related to similarities in the local order in these materials. In particular, the small distributions of η in the glasses suggest that the AsS_3 and $AsSe_3$ pyramids are well defined. This is

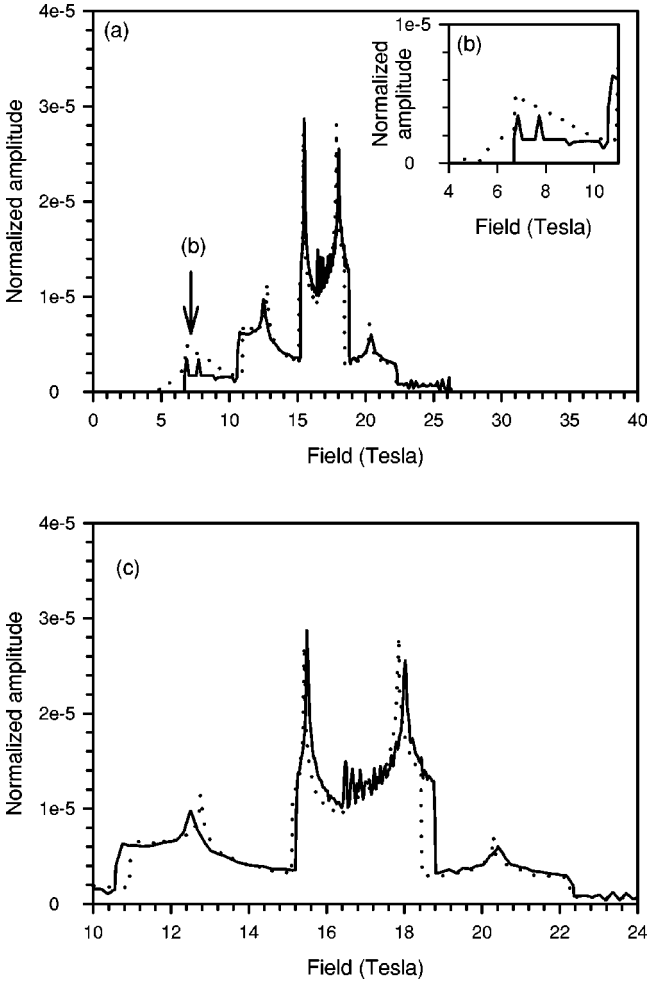

FIG. 12. Comparison of the line shapes with and without the contribution from the forbidden transitions in perturbation calculations. Here we choose $\eta=0.1$ and $s=10$. The solid lines represent the results by perturbation calculation and the dotted lines represent the results from diagonalization of the full Hamiltonian. (a) The full line shape. The arrow denotes the differences due to the contribution from forbidden transitions. (b) The central part of the line shape on an expanded scale.

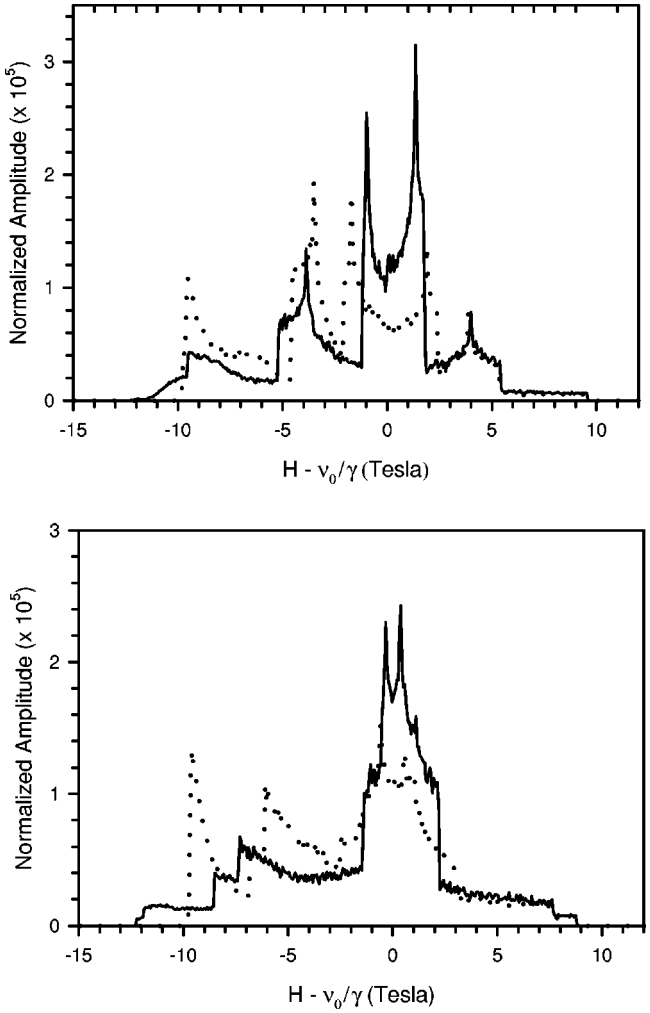

FIG. 13. Effects of multiple resonant field on the line shapes. All line shapes are simulated by diagonalizing the Hamiltonian with $\nu_{NQR}=70$ MHz. The line shapes are plotted with a rescaled field $H-\nu_0/\gamma$. (a) $\eta=0.15$, the solid line represents the line shape for $\nu_0=125$ MHz, the dotted line represents the line shape for $\nu_0=80$ MHz. (b) $\eta=0.75$, the solid line represents the line shape for $\nu_0=125$ MHz, the dotted line represents the line shape for $\nu_0=80$ MHz.

not the case for the As-rich samples, in which an overconstrained random network distorts the local bonding. We also find evidence for a statistical influence on the various bonding configurations at high As concentrations.

ACKNOWLEDGMENTS

The authors thank W. A. Harrison and M. F. Thorpe for helpful discussions. T.S. thanks A. Reyes and S. Smith for their technical support. P.H. thanks A. Kleinhammes and T. Cladwell for their support at the NHMFL. The work done at the University of Utah was supported by the NSF under Grant No. DMR-0073004. The work done at NHMFL was supported by the United States National Science Foundation through Cooperative Agreement No. DMR-0084173 and the State of Florida.

APPENDIX: COMPARISON OF EXACT DIAGONALIZATION WITH PERTURBATION THEORY

We considered the Hamiltonian $H=H_Z+H_Q$ where H_Z and H_Q are given by Eqs. (12) and (5), respectively. We further consider the case where $I=\frac{3}{2}$ (^{75}As). The quadrupole interaction depends on the materials and, therefore, can be chosen as an adjustable parameter. A parameter s is defined as

$$s=\frac{h\nu_0}{A}, \tag{A1}$$

where ν_0 is the operating frequency of the spectrometer, and A is defined as

$$A = \frac{e^2 qQ}{4I(2I-1)}. \tag{A2}$$

For $I=\frac{3}{2}$, $A=h\nu_Q/6$. The parameter s is the ratio of the characteristic Zeeman energy to the characteristic quadrupolar energy, and hence s characterizes the validity of the perturbation approach.

Several issues arise in the nonperturbation regime. First, the large quadrupole splitting of the energy levels at zero field causes a nonlinear relation between frequency and field. Even at reasonably high fields, the energy levels are offset significantly by the quadrupole splitting. Therefore, conversion from frequency dependence to field dependence is not trivial. This effect has important experimental implications, because in the experiments the field is scanned, while in the perturbation calculations the frequency shift with respect to the operating frequency is generally calculated. In the perturbation calculations, the field dependence is obtained by a linear conversion,

$$\nu = \gamma H/2\pi + \Delta\nu, \tag{A3}$$

where $\Delta\nu$ is the shift of the resonant frequency due to the local interactions. The net effect is that the field dependence, which is converted from the frequency dependence, results in a shift of the resonant line shape toward higher field. A more detailed discussion can be found in Refs. 12 and 17. To compare with experiments, the field dependence must be calculated.

A second issue is that in the nonperturbation regime, m is no longer a good quantum number. The selection rule $\Delta m = \pm 1$ is no longer valid and additional nonzero matrix elements appear. Therefore some transitions that are forbidden in the perturbation regime are now allowed. These transitions contribute additional features to the line shape. Also, for operating frequencies that are low enough, multiple resonant fields exist for the same orientation of the interaction tensors. This mechanism provides an additional contribution to the line shapes.

For the nonperturbation calculations, we choose $s=10$ and an operating frequency $\nu_0=120$ MHz. This condition closely resembles our experimental conditions. Figure 12 shows the results for $\eta=0.1$. The contribution from transitions that are forbidden in the perturbation regime can be seen at low fields in Fig. 12(b). In the central region on the spectrum, the line shape calculated by the perturbation method ($I_z=\frac{1}{2}\leftrightarrow m=-\frac{1}{2}$) is broader than that calculated by the diagonalization method [Fig. 12(c)]. The low-field discrepancy [Fig. 12(b)] is due to the large offset at zero field as discussed above. Similar behaviors are also found for other values of η. All the features of the line shapes calculated from perturbation theory are preserved in the results calculated by diagonalization, such as the additional shoulder for $\eta > \frac{1}{3}$ and the collapse of the two central divergences into a single divergence for $\eta=1$. However, significant deviations occur from perturbation theory, especially in the central portion of the spectra. Also, the contributions from the transitions that are forbidden in the perturbation regime are more prominent as the value of η increases. Specifically, for $\eta=0.6$ and $\eta=1$, an additional peak appears at lower fields that is completely missing in the results from the perturbation calculation. When the operating frequency is close to the quadrupole splitting at zero field, the effects of the multiple resonant fields begin to show up. This is clearly shown in Fig. 13. Figure 13(a) shows the simulated line shape with an NQR frequency of 70 MHz at operating frequencies of 125 and 80 MHz. The value of η is chosen to be 0.15. Figure 13(b) shows the line shape with conditions identical to those in Fig. 13(a), except the value of η is chosen to be 0.75. The field has been rescaled to eliminate the difference in the central field due to the different operating frequency. For lower operating frequency (80 MHz), an additional peak occurs at lower field (10 T below the central field). This peak persists for operating frequencies up to about 100 MHz, and disappears at higher operating frequencies.

*Email address: tnsu@physics.utah.edu

[1] J.C. Phillips, Phys. Rev. B **21**, 5724 (1979).
[2] C.J. Brabec, Phys. Rev. B **44**, 13 332 (1991), and references therein.
[3] J.P. DeNeufville, S.C. Moss, and S.R. Ovshinsky, J. Non-Cryst. Solids **13**, 191 (1973-1974).
[4] S. Ducharme, J. Hautala, and P.C. Taylor, Phys. Rev. B **41**, 12 250 (1990).
[5] M. Rubinstein and P.C. Taylor, Phys. Rev. B **9**, 4258 (1974).
[6] D.J. Treacy, P.C. Taylor, and P.B. Klein, Solid State Commun. **32**, 423 (1979).
[7] G.L. Peterson, J.G.E. Jellison, and P.C. Taylor, J. Mol. Struct. **58**, 263 (1980).
[8] Z.M. Saleh, G.A. Williams, and P.C. Taylor, Phys. Rev. B **40**, 10 557 (1989).
[9] J. Szeftel and H. Alloul, Phys. Rev. Lett. **42**, 1691 (1979).
[10] P.C. Taylor, P. Hari, A. Kleinhammes, P.L. Kuhns, W.G. Moulton, and N.S. Sullivan, J. Non-Cryst. Solids **227-230**, 770 (1998).
[11] T.P. Das and E.L. Hahn, *Nuclear Quadrupole Resonance Spectroscopy* (Academic Press, New York, 1958).
[12] P.C. Taylor, J.F. Baugher, and H.M. Kriz, Chem. Rev. **75**, 203 (1975).
[13] H. Goldstein, *Classical Mechanics*, 2nd ed. (Addison-Wesley, Reading, MA, 1980), pp. 145–148.
[14] G.H. Stauss, J. Chem. Phys. **40**, 1988 (1964).
[15] W.H.P., *et al.*, *Numerical Recipes in C: The Art of Scientific Computing* (Cambridge University Press, Cambridge, 1988).
[16] E. Palangié, C.R. Seances Acad. Sci., Ser. B **284**, 25 (1971).
[17] J. Abart, E. Palangié, W. Socher, and J. Voitlä nder, J. Chem. Phys. **78**, 5468 (1983).
[18] S.A. Dembovskii and A.A. Vaipolin, Fiz. Tverd. Tela (Leningrad) **6**, 1769 (1964).
[19] G.K. Semin, Phys. Status Solidi A **11**, K61 (1972).
[20] E.A. Kravchenko, S.A. Dembovskii, A.P. Chernov, and G.K. Semin, Phys. Status Solidi **31**, K19 (1969).
[21] T.J. Bastow and H.J. Whitfield, Solid State Commun. **11**, 1015 (1972).
[22] J.G.E. Jellison, G.L. Peterson, and P.C. Taylor, Phys. Rev. Lett. **42**, 1413 (1979).

[23] G. Balimann and P.S. Pregosin, J. Magn. Reson. (1969-1992) **26**, 283 (1977).
[24] M.F. Thorpe, D.J. Jacobs, N.V. Chubynsky, and A.J. Rader, *Rigidity Theory and Applications* (Plenum, New York, 1999), p. 239.
[25] P.C. Taylor, Z. Naturforsch **51**, 603 (1996).
[26] E. Ahn, G.A. Williams, P.C. Taylor, D.G. Georgiev, P. Boolchand, B.E. Schwickert, and R.L. Cappeletti, J. Non-Cryst. Solids **299-302**, 958 (2002).
[27] E. Ahn (unpublished).
[28] M.F. Thorpe (private communication).